RSC Advances

ROYAL SOCIETY OF CHEMISTRY

www.rsc.org/advances

Microstructures, mechanical properties and oxidation resistance of SiBCN ceramics by the addition of MgO, ZrO_2, SiO_2 (MZS) as the sintering additives

Daxin Li, Zhihua Yang*, Zhubo Mao, Dechang Jia, Delong Cai, Bin Liang, Xiaoming Duan, Peigang He, Jiancun Rao

Institute for Advanced Ceramics, Harbin Institute of Technology, Harbin 150080, China

Abstract

Nano-crystalline SiBCN ceramics were prepared by mechanical alloying (MA) plus hot pressing (HP) with the addition of MZS1 (MgO, ZrO_2 and SiO_2) and MZS2 ($ZrSiO_4$ and SiO_2) as the sintering additives. The effect of two additives on microstructures, mechanical properties and oxidation resistance of SiBCN ceramics were carefully evaluated. The addition of MZS1 and MZS2 additives in SiBCN matrix can boost elements diffusion and matrix densification. Owing to an effective densification contributed by sintering additives, the mechanical properties of SM1 and SM2 samples show an overwhelming victory than monolithic SiBCN. The oxide layers of SM1 and SM2 samples keep relatively dense and continuous, and have strong binding capacity with the matrix after oxidation testing at 1500 ^oC for 20 h. The residual of excessive carbon in SiBCN matrix should be responsible for the formation of ZrC and the outermost oxide layer structure is comprised of SiO_2 and ZrC after oxidation test. The flexural strength, Young's modulus, fracture toughness and Vicker' hardness of SM2 sample are much higher than monolithic SiBCN ceramics, reaching to 394.2 ± 41.7 MPa, 152.9 ± 16.0 GPa, 5.86±0.86 $MPa \cdot m^{1/2}$ and 8.3±0.6 GPa, respectively.

1. Introduction

SiBCN ceramics are of great interest with its combination of special structures and outstanding thermal stability up to almost 2000 ^oC, hence have attracted great attention among the researchers [1]. This ceramics normally have amorphous matrix at 1100-1400 ^oC [2], and will change to nano-ceramics with increasing temperature in inert atmosphere [3]. Recently, the methods used for fabricating SiBCN ceramics mainly include precursor-derived pyrolyzing route [4-5], mechanical alloying plus hot pressing method [6-7], physical vapor deposition (PVD, including dc magnetron co-sputtering and rf sputtering), thermal plasma chemical vapor deposition (TPCVD) and ion implantation [8-9]. At present there is no unified opinion about the microstructures of SiBCN ceramics, but it is accepted that the polymer-derived amorphous Si-B-C-N ceramics generally consist of two phases, that is, amorphous

* Corresponding author. Address: Institute for Advanced Ceramics, School of Materials Science and Engineering, Harbin Institute of Technology, P. O. Box 3022, No. 2, YiKuang Street, Harbin 150080, P. R. China. Tel: +86-451-86418792; Fax: +86-451-86414291;
E-mail address: Zhyang@hit.edu.cn

SiC_xN_{4-x} (x = 1-4) and graphite-like BN(C), 1-2 nm in size [10-12].The mechanical alloying plus hot pressing methods were studied in recent years for fabricating dense bulk SiBCN ceramics with large dimensions [13]. Yang [14] prepared amorphous SiBCN powder by mechanical alloying and subsequently applied hot pressing technique to densify SiBCN ceramics with nano-SiC and BN(C) grains uniformly distributed in the amorphous matrix. As-obtained ceramics prepared by mechanical alloying plus hot pressing have a similar microstructure compared with polymer derived SiBCN ceramics. This method has the advantage of preparing bulk ceramics with larger scale, and hence facilitating the evaluation of various mechanical properties. So far, the preparation process, microstructures and mechanical properties of SiBCN ceramics were mostly investigated, whereas less is known about the sintering ability. The poor sintering ability of SiBCN ceramics has limited its application in aerospace and aviation industries.

Some studies [15-18] have been carried out to investigate the effect of different additives on densification behavior of ceramics based composites. Results showed that special sintering additives, such as B + C, B_4C, $Al_2O_3 + Y_2O_3$ and $MgO + Al_2O_3 + SiO_2$ (MAS) promoted the sintering process effectively. In our previous research [19], the addition of 5% mol ZrO_2 or AlN in SiBCN ceramics could contribute to volume shrinkage temperature reduced to ~ 1720 ^oC and 1760 ^oC, respectively. Meantime, the relative density of SiBCN ceramics incorporated ZrO_2 or AlN additive increased to 97.7% and 96.9%, while the flexural strength reached to 575.4 MPa and 415.7 MPa, respectively. The introduction of sintering additives in SiBCN matrix had a better performance than monolithic SiBCN ceramics, especially mechanical properties and thermal stability. However, the addition of ZrO_2 or AlN would damage the oxidation resistance of SiBCN ceramics greatly because of porous oxide layer covered on oxide surface, which did not retard the oxygen diffusion into inner matrix and healed surface pores and cracks ineffectively. For this reason, other sintering additives should be explored to improve the sintering ability and oxidation resistance of SiBCN ceramics. Oxide additives were commonly applied to ceramics based composites for their outstanding sintering ability at high temperature [20]. To prepare the nano size ceramics with smaller grains and to enhance the mechanical property as well as oxidation resistance of SiBCN ceramics, we choose $MgO-ZrO_2-SiO_2$ (MZS1) and $ZrSiO_4-SiO_2$ (MZS2) as sintering additives for comparison. Therefore, it is necessary to understand the effect of sintering additives on densification behavior and oxidation resistance of SiBCN ceramics. In current work, the phase transition, microstructures, mechanical properties and oxidation resistance were evaluated carefully. The results would be helpful for further research and applications of SiBCN ceramics.

2. Experimental procedures

2.1 Raw materials and sample preparation

In current work, the used raw materials were commercially available cubic silicon (45.0 μm, 99.5 % in purity, Beijing MounTain Technical Development Center, China), hexagonal boron nitride (0.6 μm, 98.0 % in purity, Advanced Technology & Materials

Co. Ltd., Beijing, China), and graphite powders (8.7 μm, 99.5 % in purity, QingDao HuaTai Lubricant Sealing S&T Co. Ltd., China). The chemical composition was designed as Si:C:BN = 2:3:1 in molar ratio. The powder mixture was then milled for 40 h under the argon atmosphere by a planetary ball mill (P4, Fritsch GmbH, Germany) with ball to powder mass ratio set as 20:1. The rotation speed of the main disk was set as 350 rpm and the vials 600 rpm in reverse. The additives of MgO (0.3 μm, 98.0% in purity, WuXi ZeHui Chemical Co. Ltd., China), ZrO_2 (50.0 μm, 99.0 % in purity, Shenzhen Crystal Materials Co. Ltd., China), SiO_2 (38.0 μm, 99.8 % in purity, LianYunGang HuaWei Silica Powder Co. Ltd., China) were in accordance with the molar ratio of 2:5:2 by ordinary milling for 24 h with ethanol solvent, then dried in drying box at 100 ^oC. As-prepared powders were marked as MZS1. Subsequently, the MZS1 powders were sintered at 1450 ^oC to obtain bulk ceramics but were crushed to obtain another sintering additives powder, labeled as MZS2. In order to obtain a uniform distribution mixture, the amorphous SiBCN powder and sintering additives were mixed according to the mass ratio of 9:1 for 5 h by high energy ball milling. The as-milled powders were loaded into graphite dies and were heated up to 1900 ^oC with a heating rate of 20 ^oC/min , then kept at the target temperatures and under the constant uniaxial pressure (80 MPa) in the nitrogen atmosphere (1 bar) for 30 min. The loading process of the uniaxial pressure began at 1200 ^oC and ended at 1400 ^oC. In the cooling stage, furnace cooling was adopted and the uniaxial pressure was slowly unloaded in the following 5 min. The bulk ceramics prepared by sintering SiBCN amorphous powder and MZS1 additive were denoted as SM1, while SM2 presented SiBCN ceramics obtained by sintering SiBCN amorphous powder and MZS2 additive.

After sintering, the hot pressing SiBCN ceramics were diamond-ground to remove BN surface contamination. The resulting sample ceramics were cut into bars of 36 mm ×3 mm×4 mm (30 mm outer span) for measuring flexural strength and Young's modulus at room temperature by three point bending test with a crosshead speed of 0.5 mm/min. The fracture toughness was determined using the single edge notched beam (SENB) method with a crosshead speed of 0.05 mm/min. The testing bar dimensions used were 2 mm×4 mm×20 mm (16 mm outer span). The depth of the notches was 2.0 mm and the width about 0.2 mm (Instron 5569, Instron Corp., USA). The vicker's hardness (HVS-5, Laizhou, Huayin, Testing Instrument Corp., USA) was measured on polished sample surface with a load of 10 kg and a loading time of 10 s. For oxidation test, the dimensions of the polished samples were cut into 3 mm × 4 mm × 10 mm and the two major faces with 4 mm × 10 mm were ground parallel and polished with diamond lapping film. The surface roughness is about 0.5 μm. In order to avoid the influence of weight change brought by surface moisture, samples were send to an oven preset at 120^o for 10 h. Oxidation experiments were carried out in flowing air (N_2 79%，O_2 21%，steam content < 50 ppm) at 1100 ^oC, 1300 ^oC and 1500 ^oC, respectively. SM1 and SM2 samples were put into a slotted Al_2O_3 refractory brick and then send into a tube furnace (RHTH120/600/18, Nabertherm, Germany) at target temperatures. The heating rate was conducted at 5^o/min and the cooling rate was not higher than 7^o/min. The oxidation time was set as 5 h, 10 h and 20 h at target

temperatures.

2.2 Microstructures and phase transition analysis

The phases and morphologies of as-milled SiBCN powders, additive powders and their mixed powders were studied by scanning electron microscopy (SEM, 30 KV, Quanta 200 FEG, FEI Co., USA), and X-ray diffraction spectrum (XRD, 40 KV/100 mA, D/max-γB CuKa, Rigaku Corp., Japan). The structural characterization of SiBCN ceramics was analyzed using X-ray diffraction (XRD) method to obtain the X-ray diffraction spectra at $2\theta = 10^{o}$-90^{o} with the scanning speed of 4^{o}/min and the transmission electron microscope (TEM, Tecnai. F30, 300 KV, FEI Company., USA) operating at 120 kV was employed to investigate the ceramics microstructures. Elemental composition analysis was performed using the energy dispersive spectroscopy system (EDS, Oxford instruments INCAx-act, Oxforshire, U.K.) equipped in SEM.

3. Results and discussion

3.1 Densification, microstructures and mechanical properties

Fig. 1 shows the XRD patterns of SiBCN powder, sintering additives (MZS1 and MZS2), and their mixed powders. After SiBCN powder being milled for 40 h, the corresponding diffraction peaks of BN and C completely disappeared, intensities of Si peak reduced greatly and crystalline SiC is found, as indicated in Fig. 1 (a). The raw materials of MgO, ZrO_2, SiO_2 powders were milled for 24 h with ethanol solvent, the diffraction peaks of MZS1 powder corresponding to MgO, ZrO_2 and SiO_2 phases. The main peak intensity of ZrO_2 is higher than others, which may result from the high contents of ZrO_2 in raw powders, as presented in Fig. 1(b). The MZS1 additive prepared by low energy ball milling has not changed the original phases. From the diffraction peaks of MZS2 in Fig. 1 (c), the crystallization peaks are quite obvious, mainly corresponding to SiO_2 and $ZrSiO_4$.

The as-milled SiBCN amorphous powder and sintering additives (MZS 1 and MZS 2) were then mixed according to the mass ratio of 9:1 for 5 h by high energy ball milling, the corresponding XRD patterns of mixtures are shown in Fig. 1 (d) and Fig. 1 (e). The result clearly shows that the mixed powers had almost non-crystalline diffraction peaks of MZS1 powder, as indicated in Fig. (d). The possible reason for this is that the low content of sintering aids in mixture and the process of mechanical alloying (MA) adopted to prepare amorphous powder. But Fig. 1(e) displays that there still exists $ZrSiO_4$ phase in MZS2 + SiBCN powder after high energy ball milling for 5 h. The reason for this can be attributed to short time ball milling process. Mechanical alloying (MA) is an appropriate method for the preparation of various non-equilibrium materials, such as amorphous body, quasicrystal or supersaturated solid solution [6]. Ball milling time is an important parameter during MA process. If the ball milling time is long enough, the completely amorphous SiBCN + MZS2 powder could be obtained. The XRD patterns of SM1 and SM2 bulk samples produced by hot pressing at 1900 ^{o}C under a pressure of 80 MPa for 30 min in N_2 (1 bar) are displayed in Fig. 2. After hot

pressing sintering, obviously crystallized peaks are observed, and the main phases are SiC and BNC. For the low content of sintering aids, its crystallization peaks are not obvious in comparison with ceramics matrix.

Fig. 3 shows the typical SEM images of pure SiBCN ceramics. Residual pores can be clearly observed in each SEM photograph, and small cracks also exist in sample surface. The surface morphologies in Fig. 4 (a) and (c) show that the pores in as-prepared SiBCN ceramics are significantly reduced along with the residual pores becoming smaller and isolated. The ceramics particles seem to be flattered, indicating the elimination of the pores and the densification of SiBCN ceramics with the help of additives. It is generally accepted that high temperature and high pressure sintering process may accelerate plastic deformation, viscous flow and elements diffusion which facilitate ceramics densification. The addition of the two aids can low the porosity effectively in SiBCN ceramics and contribute to the densification of ceramics because of liquid phase sintering mechanism [20-23]. These results reveal that only a small amount of MZS1 or MZS2 additive could promote the sintering ability of SiBCN powder effectively, resulting from the reduction of the sintering temperature and increasing the density of bulk materials. However, few residual pores are still remained in SM2 sample and it seems to indicate a better effect on densification of MZS1 additive than MZS2 additive, as shown in Fig. 4 (d). According to the work done by F.K. van Dijen [24], SiO_2, Al_2O_3 and C additives inhibited SiC grains formation and growth effectively at an appropriate proportion. However, when C was used, the second phase was free of silica, crystalline and less weight loss during sintering was observed. Besides, the second phase is present at the triple points and no grain boundary or glassy phases are detected. R.M. German [25] established a model for supersolidus liquid-phase sintering of prealloyed powders in composites. The model used percolation concepts to create a rheological response that matched well with observations of rapid densification over narrow temperature or time ranges. This model could be used at a range of alloys and their oxides, which would be helpful for us to understand the sintering behavior of composites. M.F. Percio [26] investigated the effect of the addition of TiO_2, ZrO_2, V_2O_5 and Nb_2O_5 on the stability parameters of multi component glass. They found that the addition of any one of the oxides used as nucleants hindered the onset of crystallization and the material remained amorphous at slightly more intense heat treatments. Furthermore, the presence of ZrO_2 caused the glass to become more resistant to devitrification. A. Can [20] evaluate the densification and phase formation of liquid phase sintered silicon carbide (LPSSiC) with 10 wt.% additives by conventional hot pressing. They showed that the densification process was promoted by the addition of a small amount aids greatly due to liquid phase sintering. The mechanical properties of all the investigated SiBCN ceramics are shown in Fig. 5. As indicated, SM1 specimen has higher flexural strength than SM2 because of higher relative density. Both SM1 and SM2 samples have better performance than monolithic SiBCN ceramics, which indicating a good effect of sintering additives on densification behavior in SiBCN matrix. The flexural strength and Young's modulus were influenced greatly by porosity existence in ceramics matrix. The fracture toughness and Vicker' hardness of SM2 were 2 times

and 3 times larger than pure SiBCN ceramics, respectively. The flexural strength, Young's modulus and density of SM2 are also higher than pure SiBCN ceramics, reaching to 394.2 ± 41.7 MPa, 152.9 ± 16.0 GPa and 2.69 ± 0.1 $g \cdot cm^{-3}$, respectively. The mechanical properties of SiBCN ceramics with different additives are summarized in Table 1.

Fig. 6 and Fig. 7 presents the TEM microstructures of the SM1 and SM2 ceramics prepared at 1900 $^{o}C/80MPa/N_2$. Nano-sized BNC and SiC grains have relatively uniform distribution in the matrix without abnormal growth. The SiC grain sizes in SM1 and SM2 vary from 100 nm to 400 nm, while the grain sizes of BNC phase are much smaller than SiC and it is difficult to display BNC nano-crystal by TEM for its small size. Additionally, lots of light-and-dark strips can be found in many SiC grains, implying the existence of numerous stacking faults, as indicated in Fig. 7 (b). BNC phase mainly distributes between SiC grains or in their junction regions with no fixed shape. There are no Si_3N_4 appearing in SM1 and SM2 ceramics, which is a little different from organic polymer derived SiBCN ceramics. This may be related to the designed chemical composition, ball milling process and applied sintering techniques, requiring more research work to identify. Although the microstructures of SiC, BNC phases and their phase interface are remained further characterization, it is commonly accepted that the prepared SiBCN ceramics are composed of β-SiC and graphite like BNC and a small amount of α-SiC with the grain size of 100 nm or so [14]. The ZrO_2 in MZS1 powder could be observed in SiBCN matrix by TEM in Fig. 6, which matched with XRD results. And the selected area electron diffraction (SAD) patterns from areas A and B exhibit $[0\bar{1}\bar{1}]$ and [121] indicative of β-SiC and α-SiC structures. Other phases such as ZrC and ZrO_2 are also observed by TEM in Fig. 6(e) and (f). However, we could not find the existence of MgO and SiO_2 for their relatively low content in MZS1 additive. Fig. 7 (b) shows the detailed feathers of BNC, including its size, morphology and distribution. $ZrSiO_4$ and SiO_2 phases in MZS2 additive are hardly seen in SM2 ceramics by TEM, as shown in Fig. 7. According to the literature [27], $ZrSiO_4$ begins to decompose into ZrO_2 and SiO_2 in the range of 1450-1600 ^{o}C depending on the purity and particle size of the additive. At temperature higher than 1650 ^{o}C the reaction may accelerate many times. $ZrSiO_4$ in SM2 sample may decompose in such high sintering temperature, which matched with the XRD result. Besides, the existence of ZrO_2 may react with the excessive carbon to form ZrC. That's why we can find the existence of ZrC in SM1 and SM2 samples by TEM. In Ya.V's research [28], the use of $ZrSiO_4$ does not cause phase crystallization during fiber melt spinning, and the firber chemical composition is almost identical to the matrix. Therefore, the decomposition of $ZrSiO_4$ into ZrO_2 and SiO_2 will benefit to the phase formation instead of $ZrSiO_4$ itself. All the factors shown above state clearly that the addition of MZS1 and MZS2 additives in SiBCN ceramics could contribute to matrix densification because of liquid phase sintering mechanism.

3.2 Oxidation resistance

In order to study the oxidation behavior of SM1 and SM2 ceramics in flowing air, SM1 and SM2 samples were put into air furnace at different target temperatures (1100

°C, 1300 °C and 1500 °C) for 5 h, 10 h and 15 h. The phase transition, microstructures, and morphologies of all investigated samples were carefully studied. From the macro morphologies of SM1 and SM2 samples after oxidation test at 1100 °C for 10 h (not shown), it can be clearly seen that most regions of the samples keep integral and not visible macro-cracks are found.

In Fig. 8, the images show the surface morphologies of SiBCN ceramics after oxidation test at 1100 °C at different oxidation time (5 h, 10 h and 20 h). Surface morphology in Fig. 8 (a) shows a few cracks staggered with each other. When the oxidation temperature increases to 1100 °C for 5 h, SM1 ceramics has a thin oxide layer and only a few micro cracks propagate at local area. This indicates that the oxidation phenomenon of SM1 is not obvious at low temperature for 5 h. With the oxidation time increasing from 10 h to 20 h, SM1 ceramics samples suffer a more severe oxidation treatment, and may significantly increase the thickness of the oxide layer. However, the oxide layer still remains relatively intact and homogeneous, as displayed in Fig. 8 (c). However, small pores are observed on oxide surface of pure SiBCN ceramics at the same oxidation condition. The SEM investigations of the oxidized exterior and cross-section microstructure of SM1 sample oxidized at 1100 °C, 1300 °C and 1500 °C for 5 h are exhibited in Fig. 9. A rough and porous surface microstructure could be observed after oxidation test, as shown in Fig. 9 (a). The EDS spectra inserted in Fig. 9 (a) indicates that there still exists B_2O_3 at local area of oxide layer in comparison with Fig. 8 (a) image. With the oxidation temperature reaching to 1300 °C, lots of bubbles emerge on oxide surface of SM1 sample. At oxidation temperature of 1500 °C, bubbles disappear and cracks are found on the sample surface. The EDS results of SM1 inserted in Fig. 9 (b) and (c) shows that Si and O elements occupy a dominated position on the oxide surface. The thickness of oxide layers is changed at elevated oxidation temperature. Besides that, no distinctive feature of bonding interface between oxide layer and SiBCN matrix is discovered according to cross-section images of SM1 sample. However, the images illustrate a typical structure feature of SM1 sample after oxidation test for 5 h at various temperatures. A relatively dense oxide layer with uniform thickness adheres to ceramics matrix can be obtained from the pictures, as shown in Fig. 9 (b), (d) and (f).

Similarly to the SM1 ceramics, the surface morphologies of SM2 remain smooth, transparent and relatively dense at 1100 °C, as shown in Fig. 10 (a). However, lots of micro cracks emerge and propagate on the oxide layer and the thickness of oxide layer enhances with the oxidation temperature increasing from 1100 °C to 1500 °C. Fig. 10 (d), (e) and (f) show the fracture morphologies of SM2 at 1100 °C, 1300 °C and 1500 °C for 10 h, respectively. At 1100 °C, the thickness of the oxide layer is thinner enough with a clear boundary between SiBCN matrix and oxide layer. The oxygen distribution shows a continuous downward trend from the outermost oxide layer to the internal matrix in both samples. The elements distribution in the vicinity of the interface illustrates that the content of oxygen element in oxide layer is significantly higher than that of the matrix. The oxide layer keeps relatively dense and continuous, and has strong binding capacity with the matrix at the size of 5 μm ~ 15 μm. The mainly chemical reactions of SM1 and SM2 during oxidation test are concluded

below.

$$2\,SiC\,(s) + 3\,O_2(g) \rightarrow 2\,SiO_2\,(l) + 2\,CO\,(g) \quad (1)$$
$$C\,(s) + O_2\,(g) \rightarrow CO_2(g) \quad (2)$$
$$2\,C\,(s) + O_2\,(g) \rightarrow 2\,CO(g) \quad (3)$$
$$2\,BN\,(s) + 3/2\,O_2\,(g) \rightarrow B_2O_3(g) + N_2(g) \quad (4)$$
$$ZrSiO_4(s) \rightarrow SiO_2\,(l) + ZrO_2\,(l) \quad (5)$$
$$ZrO_2\,(s) + 2\,C\,(s) \rightarrow ZrC\,(s) + 2\,CO\,(g) \quad (6)$$
$$2ZrC\,(s) + 3\,O_2\,(s) \rightarrow 2ZrO_2\,(s) + 2\,CO\,(g) \quad (7)$$

The XRD patterns of SM1 and SM2 samples show the phase transition on oxide layers also giving support to the analysis above. After heating up to 1100 ^{o}C with a holding time for 5 h, SiO_2, BNC and ZrC can be found on the oxide layer in Fig. 11 (a). Formation of a BN(O)–SiO_2 double layer [29] during oxidation as it had been reported by Baldus et al.. However, the BN(O)–SiO_2 double layer could not be found on oxide surface of all investigated SiBCN ceramics. SiC and BNC were oxidized to form SiO_2 and B_2O_3 at 900 ^{o}C. But B_2O_3 was evaporated rapidly at 1100 ^{o}C, as a result, we could not find any diffraction peaks of B_2O_3 on oxide layer of both SM1 and SM2 samples. According to our previous analysis and senior's work [27], we believe that ZrO_2 will react with the excessive carbon to from ZrC because of carbothermal reduction reaction during oxidation test. And the remained ZrC on oxide layer of SM2 sample may result from the reaction of carbon and ZrO_2 produced by decomposition of $ZrSiO_4$. The formation process of ZrC on oxide surface can be summarized below: MZS1 additive is composed of MgO, ZrO_2 and SiO_2, while MZSs powder is consisted of SiO_2 and $ZrSiO_4$ phases. For SM1 sample, ZrO_2 would react with excessive C to form thermally stable ZrC on oxide surface. For SM2 sample, the $ZrSiO_4$ phases would decompose to ZrO_2 and SiO_2, as a result, ZrO_2 reacts with C to shape ZrC on oxide surface. However, according to B.J. Tang's work [30], they found that no trace of ZrC was observed on oxide surface after oxidation test at 1500 ^{o}C. The low content of C in $ZrSiO_4$-SiBCN(O) amorphous coating resulted in the above phenomenon. So the residual of excessive carbon in SiBCN matrix after sintering should be responsible for the formation of ZrC, as indicated in Fig. 11. In Fig. 11 (a) and (b), the content of SiO_2 in the oxide layer keeps downtrend while ZrC rises rapidly when the holding time increases from 5 h to 20 h after oxidation test. According to Michael K's [31] investigation of oxidized polymer-derived SiBCN fibers, they found that the oxidized SiBCN fibers contained three distinct concentric layers, each increasing in oxygen concentration from the core to the outer surface, which is a little different from our research shown in Fig. 9 and Fig. 10. In our current work, we find that the oxide layer can be divided into two parts according to SEM images and XRD patterns results. The first oxidation layer next to the core consisted of a mixture of nano-SiC, ZrC and turbostratic BNC, which evolved into a more oxygen-rich glass with SiO_2, ZrC and turbostratic BN grains dispersed throughout nearer the surface. However, only SiO_2 and ZrC exist on the outermost layer at 1500 °C for evaporation of B_2O_3 completely, which is different from previous research results [30]. One different point between SM1 and SM2 after oxidation test is

that the diffracted intensities of SiO_2 appears on SM1 surface oxide layer are higher than SM2 when the oxidation time reaches to 20 h at 1300 °C. Fig. 11 (c) shows the influence of temperature on oxide layer of SM2 sample with a holding time for 10 h at various target temperatures. The content of SiO_2 maintains upward trend when the temperature rises from 1100 °C to 1500 °C, and ZrC phase is also formed at 1100 °C but reaches to maximum content at 1500°C. The result is in accordance with oxide layer surface and fracture morphologies of SM2 samples. Elke Butchereit [32] prepared three precursor-derived ceramics, which were oxidized at 1300 °C and 1500 °C for times up to 100 h. They revealed that all types the scale thicknesses measured were smaller than those expected from pure SiC or Si_3N_4. As a result, SiBCN ceramics has a better oxidation resistance than monolithic SiC and Si_3N_4 prepared by the same sintering condition at high oxidation temperature.

From the above analysis and chemical reaction equation, the oxidation process of SiBCN ceramics can be divided into three stages. The weight variation of the samples as a functions of time at different temperatures are presented in Fig. 12. This will be beneficial to understand the oxidation mechanisms. In the initial stage of oxidation (~1100 °C), BNC would be oxidized to form B_2O_3 on oxide surface but was evaporated rapidly, and a small amount of SiC reacted with O to shape SiO_2. At the same time, $ZrSiO_4$ in SM2 matrix decomposed to SiO_2 and ZrO_2 along with ZrO_2 reduced to ZrC by excessive carbon. ZrO_2 in MZS1 additive also made a contribution to the formation of ZrC of SM1 sample. During oxidation tests below 1100 °C, the formed B_2O_3 might spread on the oxide surface and evaporated during heating, besides, SiO_2 spread on the surface and formed oxide layer gradually. However, before the end of B_2O_3 volatilization, the residual B_2O_3 on oxide surface and B_2O_3 form inside on the interface would react with SiO_2 to form borosilicate glass [33]. The formation of borosilicate glass would increase the melting point itself [34]. Viscosity of borosilicate was lower than that of fused silica [35]. The continuous diffusion of O could greatly thread the existing borosilicate layer easily [36]. Thereafter, the borosilicate structure on oxide layer would be destroyed completely with the volatilization of B_2O_3 at elevated temperature up to 1300 °C, which is very different from B. Lu's work [33]. In comparison with SiC and Si_3N_4 ceramics, the oxidation behavior of SiBCN ceramics is more significant at the beginning of oxidation before 1100 °C. The reasons for this should be concluded that a homogenous and continuous is formed more difficultly on oxide layer of SiBCN ceramics because the loss of boron, carbon and nitrogen occurred simultaneously. Therefore, in this stage, for all the investigated samples, weight loss was taken place significantly, as presented in Fig. 12. At a relatively low temperature, the formation of SiO_2 could not fill pores effectively on oxide layer caused by gas evaporation, as shown in reaction equation (1) - (4). This is consistent with the surface morphologies of SM1 and SM2 sample. So the SM1 and SM2 sample will be oxidized below 1100 °C with a relatively high oxidation rate, but the thickness of oxide layer is thin enough and keeps good combination with SiBCN matrix. When the oxide temperature jumps to 1300 °C, the viscosity of SiO_2 is relatively larger but still could not form a continuous and dense oxide layer on the surface of SM1 and SM2 ceramics, which resulted in a continuous

oxidation happening in matrix. However, the weight loss was alleviated effectively compared with the former. The contents of SiO_2 and ZrC increase fast along with consumption of excessive carbon and ZrO_2 in this oxidation stage. While the oxide temperature climbs to 1500 ^oC, SiO_2 with moderate viscosity will form a relatively continuous and integral oxide layer on the surface of the samples, and firmly combined with the matrix, which protects the internal materials from being oxidized [37-39]. In this stage of oxidation, in summary, pure SiC and Si_3N_4 ceramics exhibits an outstanding performance than monolithic SiBCN, SM1 and SM2 samples because of gas evaporation according to reactions (2)-(7). From Fig. 12, it seems that the weight loss phenomenon of SM1 and SM2 is more violent than pure SiBCN ceramics. This may cause by the reactions (6) and (7) due to gases evaporation. As oxidation time increases over 1500 ^oC, the oxidation resistance of SiBCN was obviously better than that of SiC and Si_3N_4 ceramics because special structures were formed on the surface of SiBCN and responsible for the excellent oxidation resistance [17, 34]. However, the formation of large amount of ZrC uniform distributed on surface can lead to crack formation and expansion. The existence of ZrC at local region will result in incomplete structure of oxide layer, and it can be predicted that a continuous oxidation behavior will take place at a low oxidation rate accompanied the entire process of oxidation, as shown in Fig. 9 and Fig. 10. The emergence and propagation of cracks on oxide layer may due to the thermal mismatch of ZrC and SiO_2 on oxide layer. Furthermore, the excessive carbon in SiBCN matrix will continue to react with ZrO_2 to form ZrC at elevated temperature for various oxidation times, meantime the reaction rate climbs rapidly with the elevation of temperature over 1500 ^oC. It is foreseeable that ZrC will disappear finally resulted from depletion of excessive carbon and oxidation of ZrC with the increasing oxidation temperature, and the oxide layer will be composed mainly of SiO_2 and ZrO_2. In our experiments, the formation of the oxide layer structure of SiBCN ceramics was not clear because of the complex phase composition. We still need to do more work on detail structures of SiBCN oxide layer, and FIB, TEM and HRTEM could be helpful.

4. Conclusions

This paper reports a study on the preparation and characterization of SiBCN ceramics with two different additives of MZS1 and MZS2. For SiBCN ceramics with the addition of different additives, SM1 has higher flexural strength than SM2 because of high relative density. However, the Young's modulus, fracture toughness and Vicker' hardness of SM2 samples perform better than SM1 samples. Both of SM1 and SM2 have a better performance on mechanical properties than pure SiBCN ceramics. The fracture toughness and Vicker' hardness of SM2 are 2 times and 3 times larger than pure SiBCN ceramics, respectively. Aids of MZS1 and MZS2 additives in SiBCN ceramics contribute to matrix densification owing to liquid phase sintering mechanism. The oxidation process of SiBCN ceramics can be divided into three stages. In the initial stage, the oxidation process is much more significant and the weight loss keeps downward trend. Due to a relatively homogenous and dense oxide layer covered on oxide surface, the weight loss rates of SM1 and SM2 samples are

retarded effectively. Sintering aids in SiBCN ceramics have a contribution to the oxidation resistance and the oxide layer remains at the size of 5 μm ~ 15 μm till 1500 ^{o}C for 20 h in flowing air. The oxide layer of SM1 and SM2 samples keep dense and continuous, and have strong binding capacity with the matrix at 1500 ^{o}C holding time for 20 h. Because of gases evaporation provided by reaction (6) and (7), the weight loss rates of SM1 and SM2 are more dramatic compared with pure SiBCN ceramics at various oxidation times of all investigated temperature. The residual of excessive carbon in SiBCN matrix should be responsible for the formation of ZrC during oxidation test. The structure of outermost oxide layer is comprised of SiO_2 and ZrC. In summary, SiBCN ceramics with MZS1 and MZS2 additives have potential to improve the mechanical properties and oxidation resistance, which may lead to the preparation of dense ceramics.

Acknowledgements

This work was financially supported by the National Natural Science Foundation of China (NSFC, Grant number 51072041, 50902031and 51021002).

References

1 R. Riedel, A. Kienzle, W. Dressler, L. Ruwisch, J. Bill, F. Aldinger, *Nature*, 1996, 382, 796.

2 M.A. Schiavon, G.D. Soraru, I.V.P. Yoshida, *J. Non-Cryst. Solids*., 2004, 348, 156.

3 R. Kumar, Y. Cai, P. Gerstel, G. Rixecker, F. Aldinger, *J. Mater. Sci.*, 2006, 41, 7088.

4 Z. Zhang, F. Zeng, J. Han, Y. Luo, C. Xu, *J. Mater. Sci.*, 2011, 46, 5940.

5 G.R. Kunmar, J. Vivekanandan, A. Mahudeswaran, P.S. Vijayanand, *Iran. Polym. J*., 2013, 22, 923.

6 Z. Yang, Y. Zhou, D. Jia, Q. Meng, *Mater. Sci. Eng., A*, 2008, 489, 187.

7 P. Zhang, D. Jia, Z. Yang, X. Duan, Y. Zhou, *J. Mater. Sci.,* 2012, 47, 7291.

8 V.M. Vishnyakov, A.P. Ehiasarian, V.V. Vishnyakov, P. Hovsepian, J.S. Colligon, *Surf. Coat. Tech.*, 2011, 206, 149.

9 A. Vijayakumar, R.M. Todi, V.O. Todi, K.B. Sundaram, *J. Electrochem. Soc*., 2007, 154, 875.

10 J. Haug, P. Lamparter, M. Weinmann, F. Aldinger, *Chem. Mater.*, 2004, 16, 83.

11 J. Schuhmacher, F. Berger, M. Weinmann, J. Bill, F. Aldinger, K. Muller, *Appl. Organomet. Chem*., 2001, 15, 809.

12 N. Liao, W. Xue, H. Zhou, M. Zhang, *RSC Adv.*, 2013, 3, 14458.

13 P. Zhang, D. Jia, Z. Yang, X. Duan, Y. Zhou, *Ceram. Int*., 2013, 39, 1963.

14 Z. Yang, D. Jia, Y. Zhou, J. Zhang, *Mater. Sci. Eng., A*, 2008, 448, 241.

15 J. M. Bind, J.V. Biggers, *J. Am. Ceram. Soc*., 1975, 58, 304.
16 D.H. Kim, C.H. Kim, *J. Am. Ceram. Soc*., 1990, 73, 1431.
17 B. Lu, Y. Zhang, *Mater. Lett*., 2014, 137, 483.
18 J. Han, Y, Song, X. Liu, F. Wang, *RSC Adv.*, 2014, 4, 51995.
19 P. Zhang, D. Jia, Z. Yang, X. Duan, Y. Zhou, *J. Alloy. Compd*., 2012, 537, 346.
20 A. Can, M. Herrmann, D.S. Mclachlan, I. Sigalas, J. Adler, *J. Eur. Ceram. Soc.*, 2006, 26, 1707.
21 S.N. Perevislow, *Glass. Ceram*., 2013, 70, 265.
22 F. Yan, F. Chen, Q. Shen, L. Zhang, *Key, Eng. Mater*., 2007, 336, 1062.
23 R. M. German, P. Suri, S. J. Park, *J. Mater. Sci.*, 2009, 44, 1.
24 F. K. van Dijen, E. Mayer, *J. Eur. Ceram. Soc*., 1996, 16, 413.
25 R.M. German, *Metall. Mater. Trans., A*, 1995, 26a, 279.
26 M.F. Percio, S.D.D. Campos, R. Schneider, E.A.D. Campos, *J. Non-Cryst. Solids.*, 2015, 411, 125.
27 A. Kaiser, M. Lobert, R. Telle, *J. Eur. Ceram. Soc.*, 2008, 28, 2199.
28 Ya.V. Lipatov, S.I. Gutnikov, M.S. Manylov, E.S. Zhukovskaya, B.I. Lazoryak, *Mater. Des*., 2015, 73, 60.
29 H.P. Baldus, G. Passing, *Mater. Res. Soc. Symp. Proc.*, 1994, 346, 617.
30 B. Tang, Z. Feng, S. Hu, Y. Zhang, *Appl. Surf. Sci.*, 2015, 331, 490.
31 M.K. Cinibulk, T.A. Parthasarathy, *J. Am. Ceram. Soc*., 2001, 84, 2197.
32 E. Butchereit, K.G. Nickel, *J. Am. Ceram. Soc*., 2001, 84, 2184.
33 B. Lu, Y. Zhang, *Ceram. Int*., 2015, l41, 1023.
34 K.G. Nickel, E. Butchereit, C. Schumacher, *J. Electrochem. Soc.*, 2000, 99, 365.
35 E.L. Bourhis, G. Patriarche, *Phys. Status. Solidi. C*, 2009, 6, 1846.
36 J.W. Fergus, W.L. Worrell, *J. Am. Ceram. Soc*., 1995, 78, 1961.
37 J.R.G. Ervin, *J. Am. Ceram. Soc.*, 1958, 41, 347.
38 D.S. Fox, *J. Am. Ceram. Soc.*, 1998, 81, 945.
39 C.G. Cofer, J. Economy, *Carbon*, 1995, 33, 389.

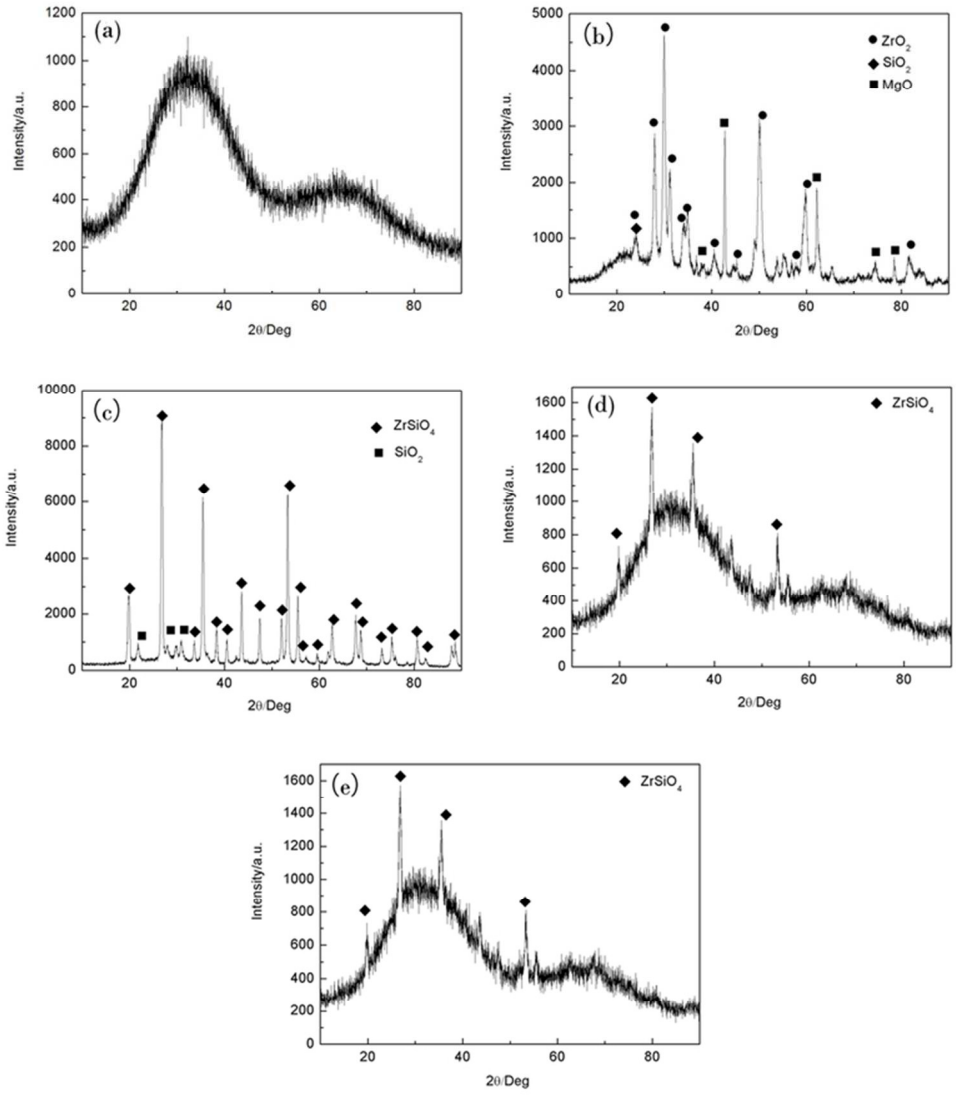

Fig. 1 XRD patterns of the raw materials. (a) SiBCN powder, (b) MZS1 powder, (c) MZS2 powder, (d) MZS1+ SiBCN powder, (e) MZS2+ SiBCN powder.
33x37mm (600 x 600 DPI)

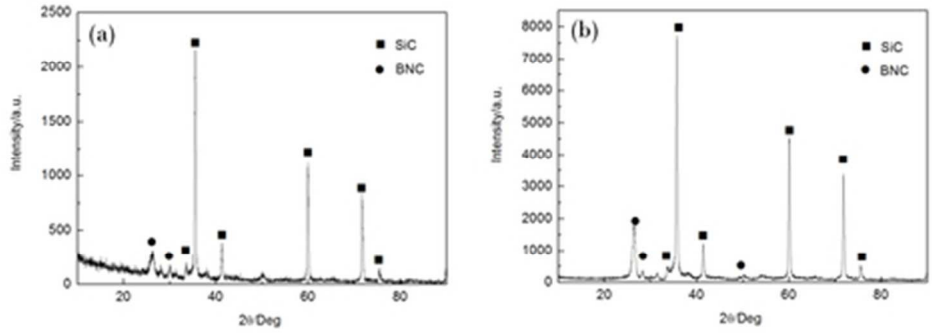

Fig. 2 XRD patterns of SM1 and SM2 bulk samples produced by hot-pressed at 1900 oC/80MPa. (a) SM1 sample, (b) SM2 sample.
20x8mm (600 x 600 DPI)

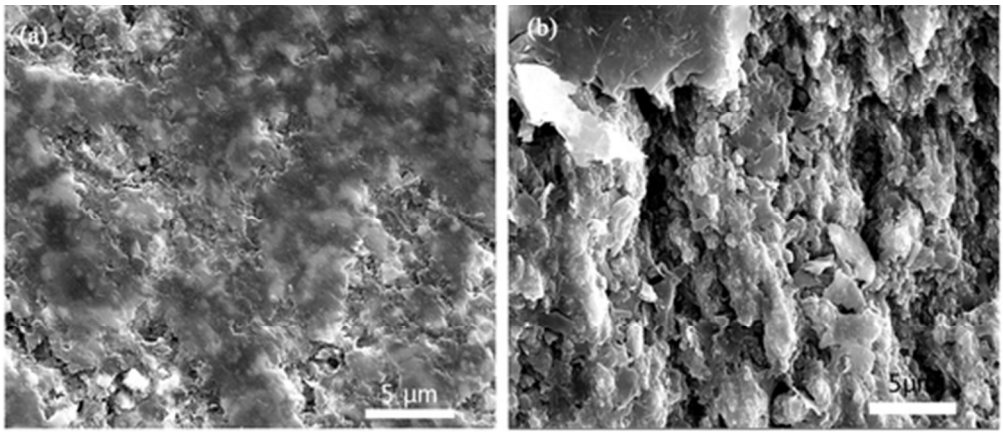

Fig. 3 SEM surface and fracture images of pure SiBCN ceramics hot-pressed at 1900 oC/80 MPa. (a) Surface morphology, (b) fracture morphology.
21x9mm (600 x 600 DPI)

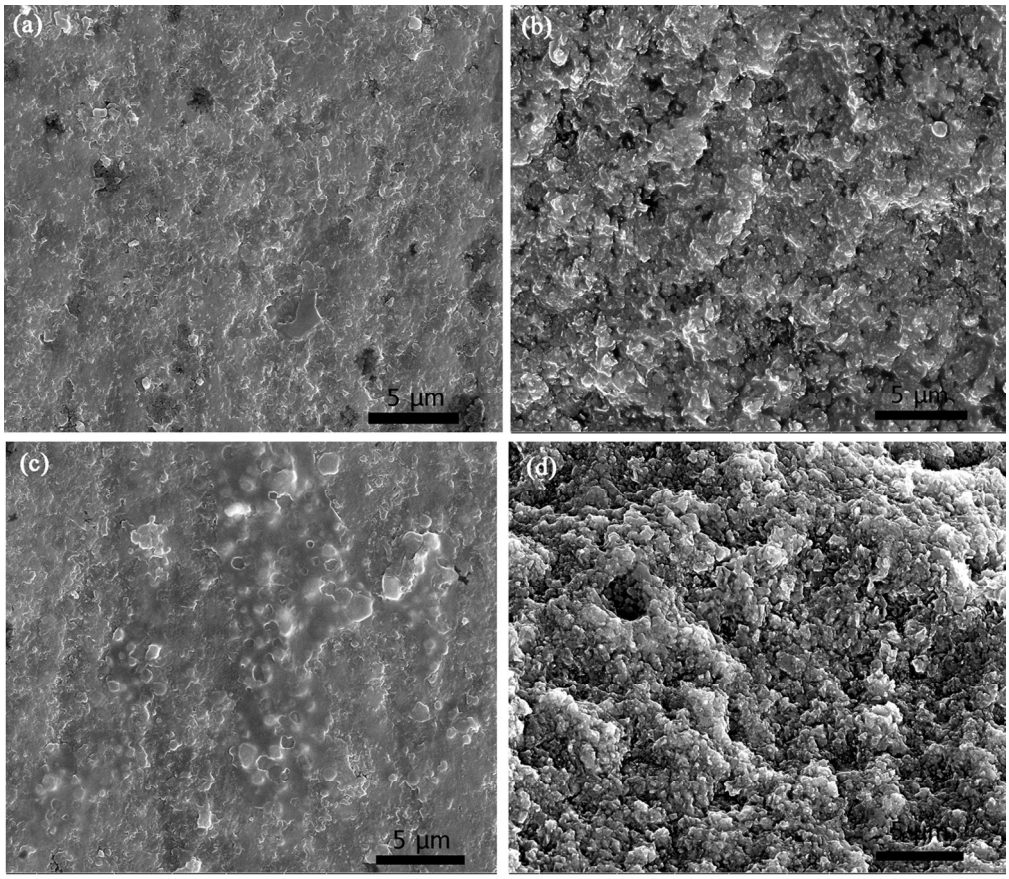

Fig. 4 SEM surface and fracture images of SM1 and SM2 ceramics hot-pressed at 1900 oC/80 MPa. (a) (b) SM1 sample, (c) (d) SM2 sample.

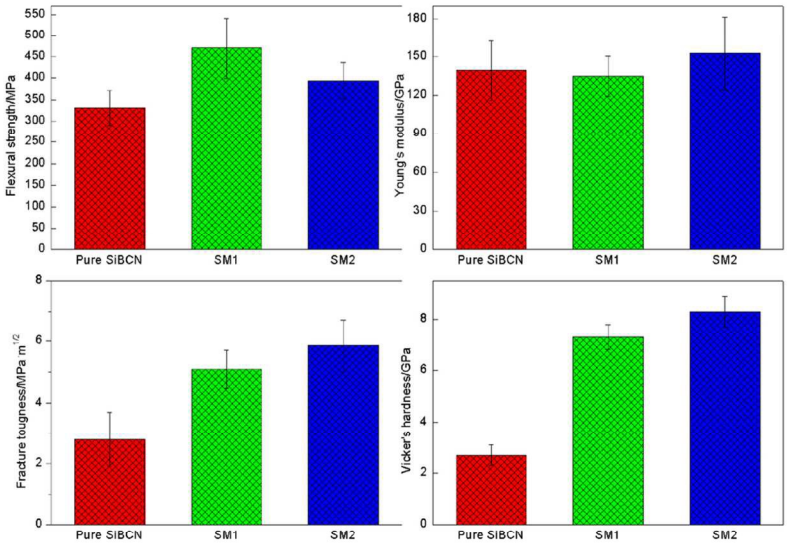

Fig. 5 Mechanical properties of all the investigated SiBCN ceramics.
53x36mm (600 x 600 DPI)

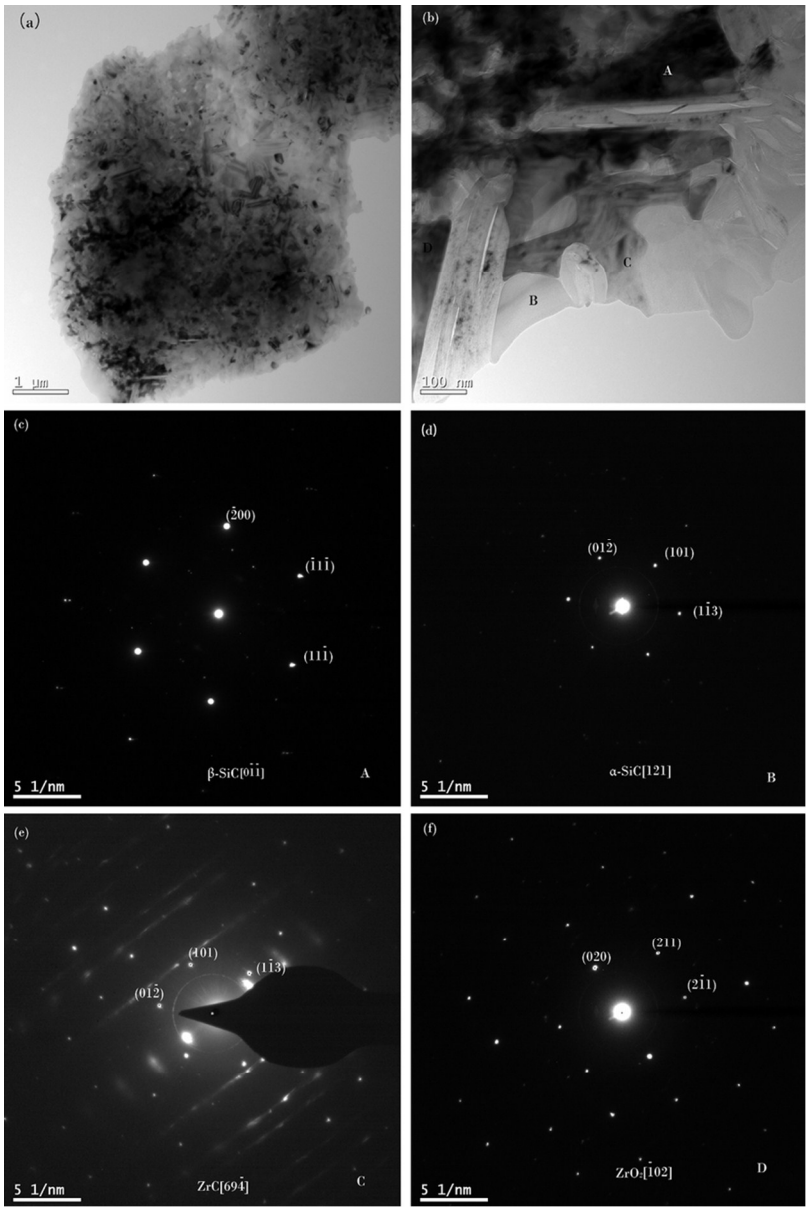

Fig. 6 Structural features of the as-prepared SM1 ceramics hot-pressed at 1900 oC /80MPa.
(a) Bright field image showing the morphologies of SM1, (c) (d) (e) (f) SAD pattern of corresponding region A, B, C, D in (b).

38x57mm (600 x 600 DPI)

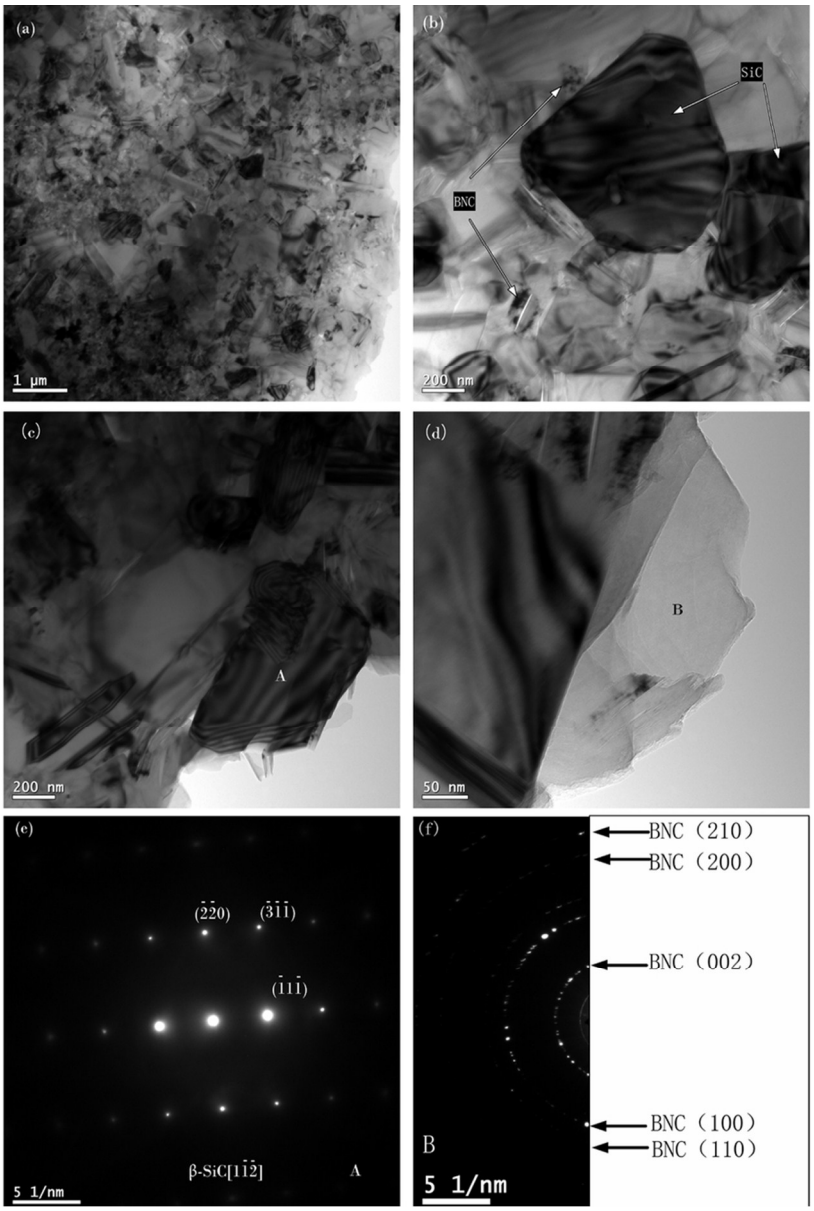

Fig. 7 Structural features of the as-prepared SM2 ceramics hot-pressed at 1900 oC/80MPa.
(a) Bright field image showing the morphologies of SM2 sample, (b) SiC and BNC phases, (e) SAD pattern of region A in (c), (f) SAD pattern of region B in (d).

37x55mm (600 x 600 DPI)

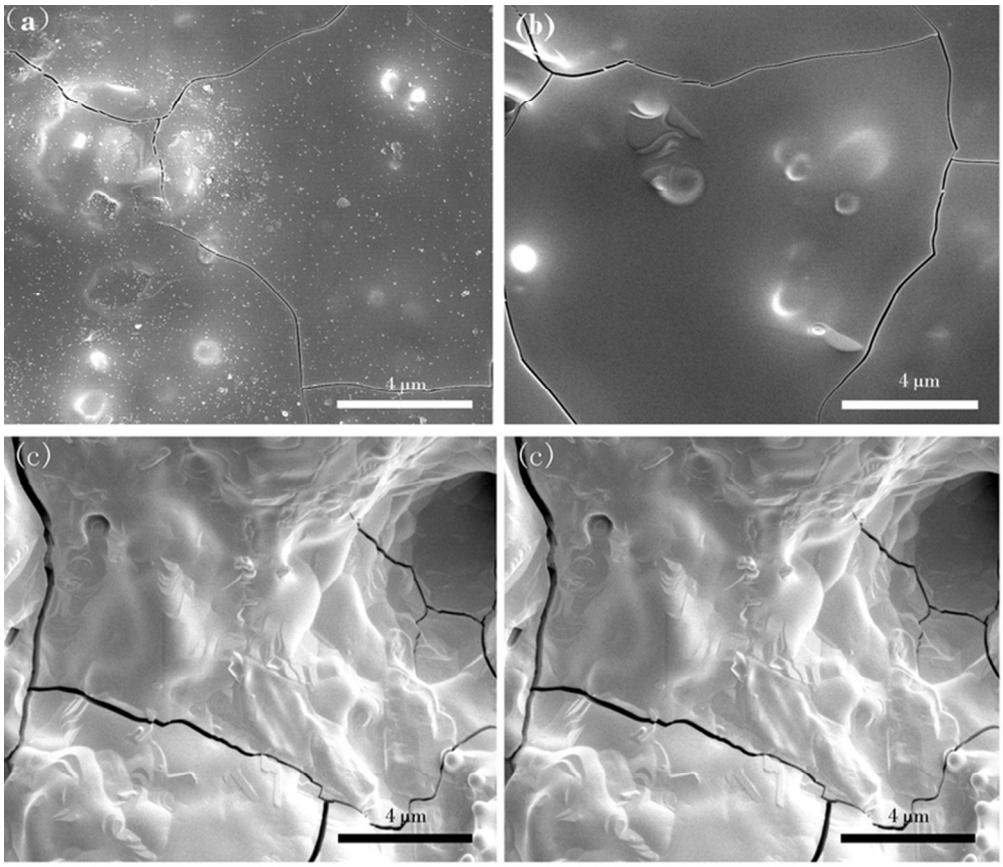

Fig. 8 Surface morphologies of SiBCN ceramics after oxidation test at 1100 oC at different oxidation time. (a) SM1 5 h, (b) SM1 10 h, (c) SM1 20 h, (d) pure SiBCN 20 h.
32x28mm (600 x 600 DPI)

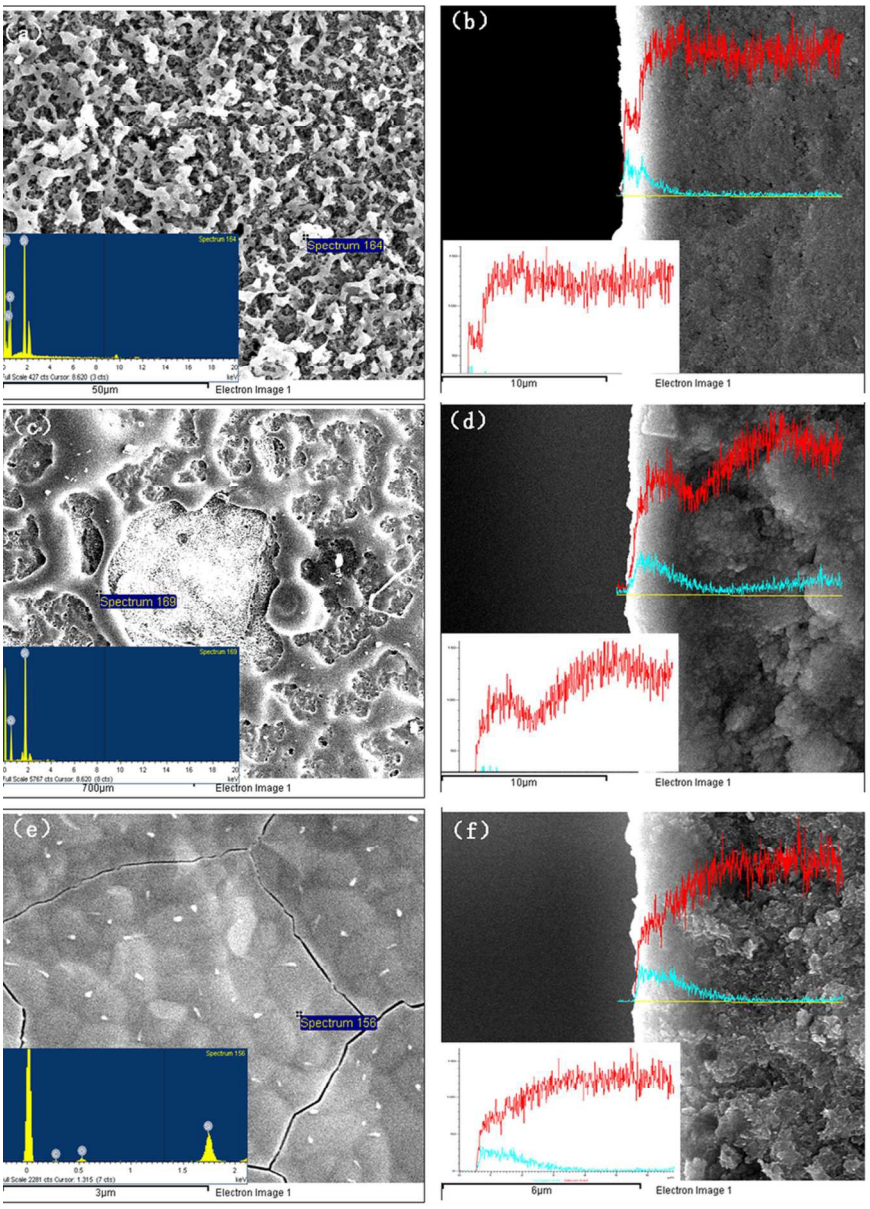

Fig. 9 Surface and fracture morphologies of SM1 ceramics after oxidation test for 5 h at different temperatures. (a) (b) 1100 oC, (c) (d) 1300 oC, (e) (f) 1500 oC.
42x58mm (600 x 600 DPI)

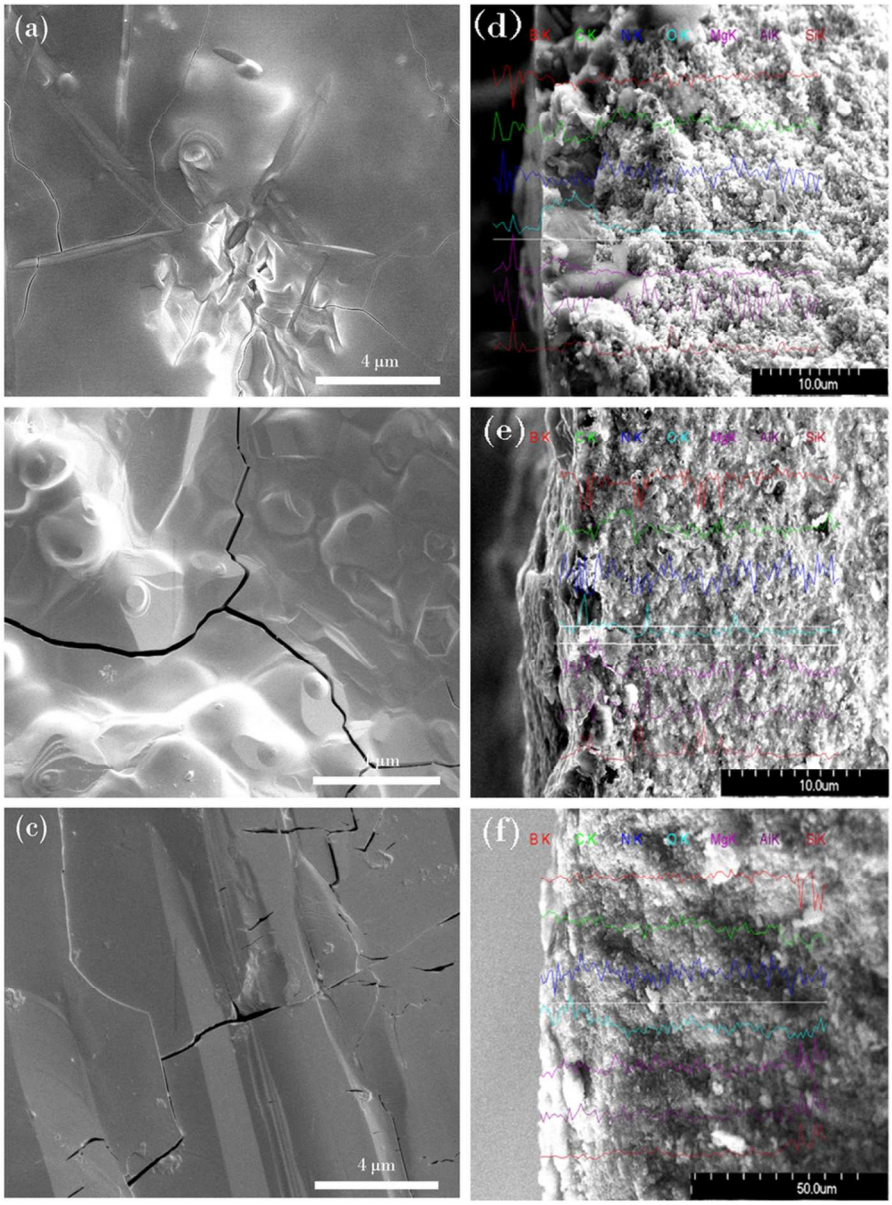

Fig. 10 Surface and fracture morphologies of SM2 ceramics after oxidation test for 10 h at different temperatures. (a) (d) 1100 oC, (b) (e) 1300 oC, (c) (f) 1500 oC.
40x54mm (600 x 600 DPI)

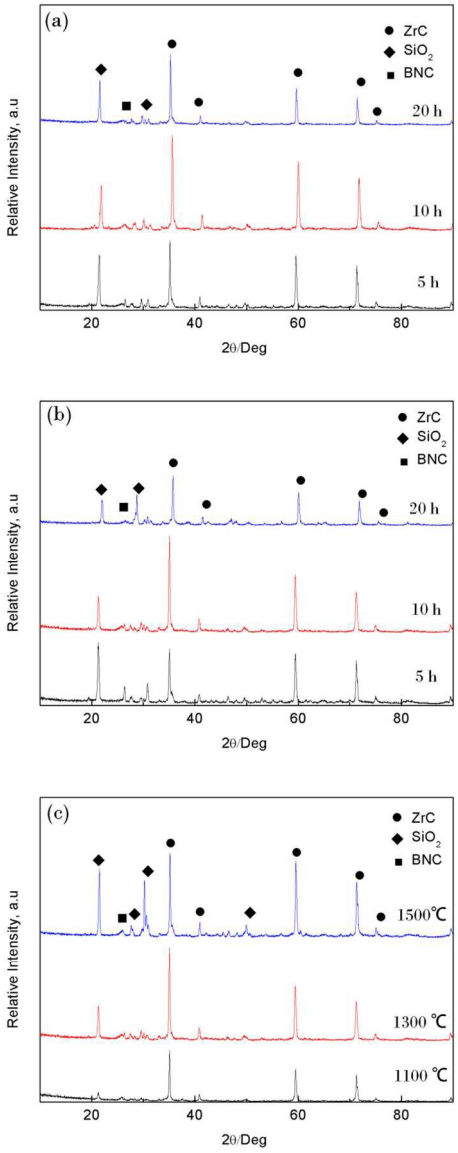

Fig. 11 XRD patterns of the SM1 and SM2 ceramics after heat treat in air at different temperatures with various oxidation time. (a) SM1 after heat treat in air at 1300 oC, (b) SM2 after heat treat in air at 1300 oC, (c) SM2 after heat treat for 10 h.
48x116mm (600 x 600 DPI)

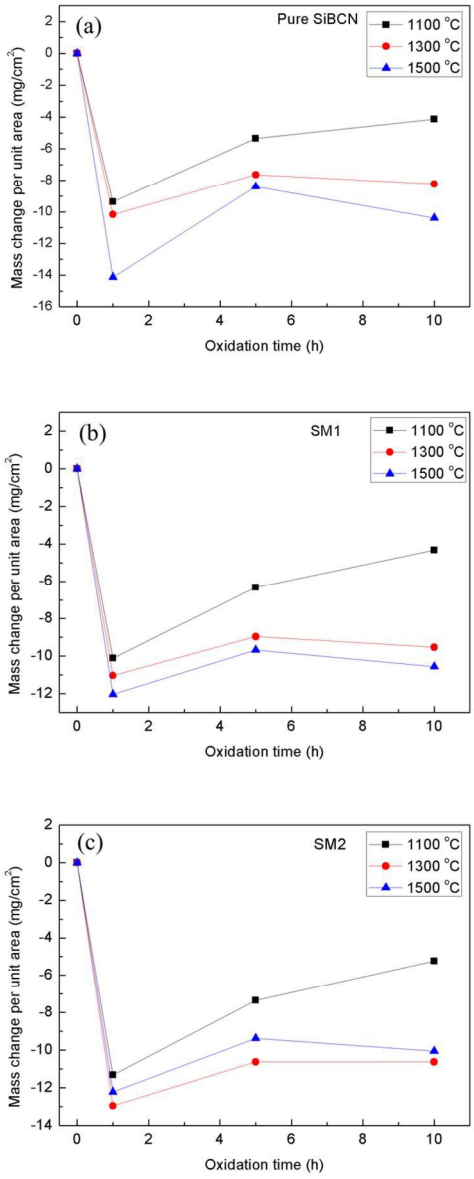

Fig. 12 The weight variation of the samples as a functions of time at different temperatures. (a) Pure SiBCN sample, (b) SM1 sample, (c) SM2 sample.

47x112mm (600 x 600 DPI)

Table 1 The effect of different additives on the density and mechanical properties of SiBCN ceramics

sample	Flexural strength/MPa	Young modulus/GPa	Fracture toughness/MPa·$m^{1/2}$	Vicker' hardness/GPa	Density /g·cm^{-3}
Pure SiBCN	331.1±40.5	139.4	2.80±0.90	2.7±0.4	2.60±0.01
SM1	470.4±71.1	134.9	5.10±0.62	7.3±0.5	2.78±0.01
SM2	394.2±41.7	152.9	5.86±0.86	8.3±0.6	2.69±0.01

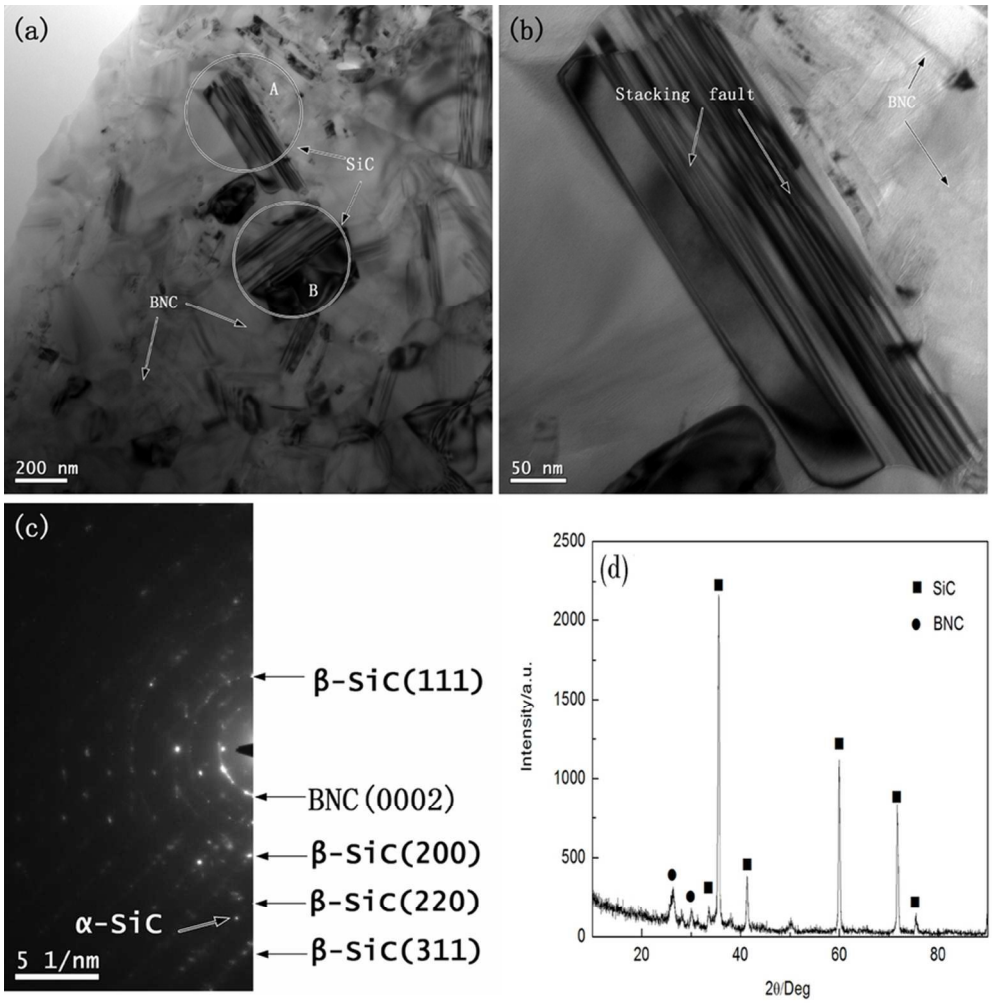

Textual abstract: Owing to an effective densification contributed by sintering additives, the mechanical properties of SM1 and SM2 show an overwhelming victory than monolith.
40x40mm (600 x 600 DPI)